Energy Conversion and Management 348 (2026) 120752

Contents lists available at ScienceDirect

Energy Conversion and Management

journal homepage: www.elsevier.com/locate/enconman

Combined cooling for CSP plants: Modeling, experimental validation and optimization analysis

Juan Miguel Serrano [a], Patricia Palenzuela [a], Javier Ruiz [b], Pedro Navarro [b], José Muñoz-Cámara [b], Bartolomé Ortega-Delgado [c], Lidia Roca [a,*]

[a] CIEMAT-Plataforma Solar de Almería-CIESOL, Ctra. de Senés s/n, Tabernas, Almería, 04200, Spain
[b] Miguel Hernández University of Elche, Avda. de la Universidad, s/n, Elche, 03202, Spain
[c] Department of Energy Engineering, University of Seville, Camino de los Descubrimientos s/n, Seville, 41092, Spain

ARTICLE INFO

Dataset link: 10.5281/zenodo.17312546

Keywords:
Concentrated solar power
Water consumption
Wet cooling tower
Air cooled heat exchanger
Hybrid cooling

ABSTRACT

The global development of Concentrated Solar Thermal Power (CSP) projects demands new technologies that enhance the thermal efficiency of power cycles without increasing costs or environmental impact. Among the subsystems of the power cycle, the cooling circuit plays a critical role, as it must minimize water consumption while maintaining high efficiency; a challenge that is particularly relevant in arid regions where many CSP plants are installed.

This paper presents a model for a cooling system that combines Dry Cooling (DC) and Wet Cooling Tower (WCT) technologies, enabling multiple operating configurations (parallel, series, parallel–series, only-WCT, and only-DC). The model was validated using experimental data from a 200 kW_{th} pilot plant, achieving a Mean Absolute Error (MAE) below 0.97 °C for system temperatures and 19.4 l/h for water consumption.

An optimization analysis was also performed, demonstrating the potential of the proposed technology to provide adaptive cooling for CSP plants under varying seasonal and operating conditions. For the pilot plant during summer, optimally combining DC and WCT in a parallel series configuration enabled a nearly continuous variation in specific electricity consumption, ranging from 0.06 kW_e/kW_{th} in only-DC operation to values up to 90 % lower in only-WCT mode, at a water usage cost of 1.48 l/kWh_{th}.

1. Introduction

The global energy landscape is currently undergoing a significant transition, shifting from traditional fossil fuels to a greater reliance on renewable energy sources like solar, wind, and hydro.

Among renewable energy sources, Concentrated Solar Power (CSP) stands out due to its inherent capacity for energy storage at lower costs, enabling the dispatchability of electricity even in the absence of direct solar irradiation. This feature provides CSP with a distinct advantage over variable-output renewables such as photovoltaic and wind energy that depend on expensive storage (*i.e.*, batteries), which allow grid stability and reduce the need for auxiliary backup systems. Spain is currently a global leader in CSP technology, with an installed capacity of 2.3 GW_e in 2025 and is expected to reach 4.8 GW_e by 2030 according to the Spanish National Integrated Energy and Climate Plan (PNIEC).

However, in order to significantly boost the development of CSP technology, it is essential to increase the efficiency of the plants to improve their cost competitiveness. Their efficiency is strongly influenced by the condensing temperature at which the steam is condensed. Two primary strategies are employed for condensation heat rejection: wet cooling and dry cooling. Wet cooling towers (WCT) typically allow for lower condensation temperatures, close to ambient wet-bulb temperature, leading to improved cycle efficiency and higher power output. However, this approach demands substantial water consumption to compensate for evaporative, drift, and blowdown losses. Dry cooling (DC) systems, on the other hand, operate using ambient air as the heat sink. Although they eliminate the need for water, their thermal performance is reduced, especially at high ambient temperatures, and have a higher associated electric energy consumption. These systems can be classified as either direct or indirect [1]. In direct systems, steam is delivered directly to an Air Cooled Condenser (ACC), where heat is rejected to the environment in a single step. Condensation occurs inside finned tubes as ambient air flows across the external finned surfaces, which are typically arranged in an A-frame (forced draft) or delta (induced draft) configuration. In indirect systems, steam first condenses in a separate condenser, and the resulting warm cooling water is then

* Corresponding author.
E-mail address: lidia.roca@psa.es (L. Roca).

https://doi.org/10.1016/j.enconman.2025.120752
Received 31 August 2025; Received in revised form 21 October 2025; Accepted 6 November 2025
Available online 13 November 2025

Nomenclature

C	electrical or water consumption (kW, l/h)
c	constant in ASHRAE correlation
c_p	specific heat (J kg^{-1} K^{-1})
D	diameter (m)
h	enthalpy (J kg^{-1})
HR	relative humidity (%)
h_i	convective heat transfer coefficient for the internal fluid (W m^{-2}K^{-1})
h_o	convective heat transfer coefficient for the external fluid (W m^{-2} K^{-1})
k	thermal conductivity (W m^{-1} K^{-1})
L	length (m)
Le	Lewis number
m	constant in ASHRAE correlation
$\dot{m}$	mass flow rate (kg s^{-1})
Me	Merkel number
n_{tb}	number of tubes
$\dot{Q}$	thermal power (kW)
q	volumetric flow rate (m^3 h^{-1})
R	distribution ratio (%)
R_i	internal fouling resistance (m^2 K W^{-1})
R_o	external fouling resistance (m^2 K W^{-1})
T	temperature (K)
U	heat transfer coefficient (W m^{-2} K^{-1})
w	frequency level of the fan (%)

Greek symbols

ρ	density (kg m^{-3})
ω	humidity ratio (kg kg^{-1})

Subscripts

a	air
amb, ∞	ambient conditions
c	surface condenser
cc	combined cooler
$cond$	condensate
dc	dry cooler
e	electrical power
i	inner
in	inlet
o	outer
out	outlet
p	parallel component
s	saturated, series component
tb	tube
v	vapor
w	water
wct	wet cooling tower

Abbreviations

ACC	Air Cooled Condenser
ACHE	Air Cooled Heat Exchanger
CC	Combined Cooling systems
CSP	Concentrated Solar Power
DC	Dry Cooling
DoE	Design of Experiments
HC	Hybrid Cooling systems
LMTD	Log Mean Temperature Difference
MAE	Mean Absolute Error
MAPE	Mean Absolute Percentage Error
NLP	Non Linear Programming
PSA	Plataforma Solar de Almería
SC	Surface Condenser
LCOE	Levelized Cost Of Energy
TL	Thermal Load
WCT	Wet Cooling Tower

circulated through an Air Cooled Heat Exchanger (ACHE) for final heat rejection to the atmosphere.

Hybrid cooling systems (HC) (which integrate dry and wet cooling methods into the same tower) and combined cooling (CC) (which consist of separate dry and wet cooling devices) are attracting growing attention because of their potential to tackle the problems of conventional ones. The potential of these alternative cooling systems has been already proven in several research works published in the scientific literature, both in conventional and solar thermal power plants. In [1], a comparison between conventional and alternative cooling systems was carried out in terms of water consumption. The comparison was made by a theoretical study and for five different locations of a conventional power plant and different cooling systems: a direct dry cooling system (type ACC), a WCT and a CC consisting in a WCT in parallel with an ACC. The results showed that the CC option system achieved a water consumption reduction between 15 % and 85 % compared to the conventional only-WCT. For reductions below 15 %, deluged condensers or inlet spray pre-cooling become the more suitable options. The same authors carried out the comparison between the same alternative and conventional cooling systems but this time in terms of cost, water use, and performance trade-offs [2]. They concluded that the ACC eliminates water use but increases costs by 2.5–4x and reduces efficiency by 5–7 %, being thus only viable either in extreme water-scarce regions or if water prices rise significantly. On the other hand, it was concluded that the CC system reduces water use by 40–75 %, with a 1.9–2.8x cost increase and a 2 % efficiency loss. Performance depends strongly on climate, being most favorable in arid regions with extreme climates (72 % reduction at 1.9x cost) and least favorable in hot, arid conditions (39 % reduction at 2.8x cost). Tang et al. [3] developed a simulation model for a conventional power plant that uses the combination of dry (type ACC) and WCT based on a real 300 MW_e power plant located in China. They analyzed the performance of the plant at different cooling configurations and under varying conditions of ambient temperature, relative humidity, and heat load. The results were successfully validated against experimental data obtained from the real plant, and, among the main conclusions, they highlighted the limitations of using only ACC to maintain the exhaust pressure at higher ambient temperatures, affecting strongly the plant performance. A gap of this study is that they did not evaluate the water and electricity consumption.

In [4], the study considers a 107 MW_e non-renewable cogeneration plant located in Northern Italy, which also has a CC composed of a WCT in parallel with an ACC. They developed a model using Thermoflex, based on the same configuration of that plant, which was validated against plant manufacturer data and real plant performance over an extensive range of operating conditions. The study analyzed how to maximize the power generated optimizing the condensation system for the case of CC and only-ACC. Since the analysis did not include the evaluation of the water consumption, the best configuration was in general only-WCT, although a change in the plant configuration from CC to only-ACC was recommended to maximize the net power output when the district heating demand is very high and the ambient temperature is below 15 °C. A different CC configuration was analyzed

in [5]: an ACHE arranged in series with a WCT. They developed a model of a conventional 660 MW_e thermal power plant with the CC system to evaluate the thermal performance as well as water and power consumption, under three operating modes (ACHE, WCT and CC) considering variations in ambient temperature and relative humidity; however, no model validation is reported. Simulation results suggest assigning a greater share of the cooling load to the dry section under relatively low ambient temperatures to reduce the water consumption. Conversely, at higher ambient temperatures, increasing the proportion of the load handled by the wet section is recommended to lower turbine exhaust pressure to improve power generation efficiency.

In the case of CSP plants, there are also several studies in the scientific literature dealing with the evaluation of the impact of alternative cooling systems on plant performance and water consumption [6–9]. In [6] different cooling systems were evaluated theoretically for a 35 MW_e CSP plant using Solar Advisor Model (SAM) and IPSEpro for the modeling of the solar field and power block, respectively. They compared dry cooling (using ACC) and CC (composed of ACC in parallel with a WCT) with respect to the traditional WCT in CSP. In the case of the CC two configurations were studied in terms of thermal load going to the WCT and to the ACC, respectively: 85/15 % and 50/50 %. Results proved the potential of these systems by a clear trade-off between water savings and efficiency. In the case of the CC system 85/15, a 85 % of water reduction was achieved with a 2.3% in efficiency loss. In the case of the CC system 50/50 the water consumption was reduced by 52 % with only a 1.7 % in efficiency loss. Another different CC system integrated into a CSP plant was evaluated in [7]. The model was developed in Thermoflex and the CSP plant was based in the same configuration as the 50 MW_e CSP plant Andasol I (located in Spain) that uses WCT. The study compared the performance and water consumption of this CSP plant with respect to the one using CC system composed of ACHE and WCT arranged to operate either in series or in parallel configurations. The results obtained from the simulations showed that the series-parallel configuration provided the greatest water savings, achieving up to a 50 % reduction in water consumption compared to the only-wet cooling option, while allowing a 2.5 % increase in power generation relative to the only-dry configuration. In contrast, the parallel configuration offered the highest power output, with a 3.2 % increase compared to the only-dry case, along with a 30 % reduction in water use compared to the only-wet option. The CSP plant Andasol I was also taken as a reference case in [8]. In this case, the CSP plant was modeled using EES software and three cooling systems were considered: a WCT, a dry cooling system (type ACC) and a HC based on an ACC with a wetted-media pad evaporative pre-cooling. The analysis was focused on the evaluation of the water use, the ambient temperature effect and the annual water consumption and energy production. The results obtained indicated that energy production is 12.60% higher for WCT and 4.65 % higher for HC compared to the case that uses the ACC. Additionally, the HC system achieves 71.74 % of the water consumption reduction compared with the case of using a WCT, with a 7.06 % reduction in power production. The integration of other HC systems into Andasol I CSP plant was investigated in [9]. They evaluated theoretically the integration of a Natural Draft Dry Cooling Tower (NDDCT) and a pre-cooled NDDCT system as innovative heat rejection solutions for the CSP plant, and compared their performance and water consumption with conventional alternatives, including Mechanical Draft Wet Cooling Towers (MDWCT), ACC, and a HC consisting of a pre-cooled ACC system that uses media pads and spray nozzles. They developed analytical models for the cooling systems and their interaction with the CSP plant and validated the models against results reported in the literature. The results showed that the pre-cooled NDDCT is the most efficient option in terms of water consumption per unit of energy generated (only 2.9 % less efficiency compared to MDWCT with 76.7 % less water usage than MDWCT). Among CSP research works focused on the cooling part, some works considered the impact of the alternative systems on the costs. Mdallal et al. [10] optimized the design of a CSP plant in terms of levelized cost of energy (LCOE) and annual energy production. For that, they developed a response surface model of the CSP plant based on the results obtained from two software tools: SAM and Design-Expert. The study compared different cooling systems: WCT, ACC and a CC system based on an ACC in parallel with a WCT. From the results obtained, it can be highlighted that the CC is the most cost-effective cooling technique and has the highest energy output compared to the evaporative and air-cooling methods. Concretely, the highest energy production ($3.44 \cdot 10^8$ kWh) was obtained with this CC system with an acceptable LCOE (19.31 €/kWh). In [11], a model of a CSP located in China is presented, which consider the integration of two possible cooling system: an ACC and a CC system composed of a ACC in parallel with a WCT. They analyzed the annual operation and the LCOE and revenues of the CSP plant for both dry and CC systems, considering different number of ACCs and wet cooling towers. Results showed that CC offers a more favorable LCOE at low ratios of the price of water to electricity. However, when this ratio is 10 or higher, the option of using ACC without WCT becomes the most recommended one.

Despite the already proved potential of HC/CC systems, their deployment remains very limited. The only commercial CSP plant known to employ this technology (ACC and WCT in parallel) is the Crescent Dunes Solar Energy Project, a 110 MW_e facility equipped with 1.1 GWh of molten-salt thermal energy storage [12]. There are also some lab and pilot-scale projects that allow the evaluation of this kind of systems. At lab-scale, Asvapoositkul et al. [13] show the case of HC system composed of a WCT with a DC section. They developed a simulation model based on the configuration of the lab-scale facility and compared experimental data with simulation results. At pilot scale, a HC based on an air-cooled deluge condenser was successfully built and tested in Stellenbosch, South Africa [14] within the European project *MinWaterCSP*. Another pilot-scale facility is the one located at PSA, that is the only one that allows the evaluation of CC systems. The authors of this work have already addressed advanced research on this pilot plant, presenting an exhaustive experimental work [15] and the model and validation of one of the components (e.g. the wet cooling tower) [16]. In the present paper, to the best knowledge of the authors, we present the first thoroughly detailed model of the complete CC system composed of a WCT and an ACHE in series and parallel configurations, which is also validated with experimental data from the pilot plant.

The main contributions of this work are as follows:

- Develop a physics-based model for a combined cooling (CC) system with WCT and ACHE-type DC in multiple configurations (parallel, series, parallel–series, only-WCT, only-DC), validated for the first time with experimental pilot-plant data.
- Collect and analyze an extensive experimental dataset covering diverse ambient conditions and thermal loads, improving on previous limited validations.
- Perform multi-objective optimization of electricity and water consumption using the validated physics-based model, enabling system studies at any scale without relying on large datasets or risking extrapolation.

The paper is structured as follows: Section 2 includes the description of the facility where the experimental tests were conducted, the mathematical modeling is presented in Section 3 and the experimental procedure in Section 4. Section 5 presents the calibration and validation of the models, and Section 6 analyzes the operation optimization under different case study scenarios. Finally, Section 7 summarizes the main findings and includes recommendations for future research.

2. Combined cooling pilot plant

The combined cooling pilot plant at Plataforma Solar de Almería (see Fig. 1) is a unique facility that integrates a wet cooling tower and a dry cooler in a flexible hydraulic configuration. It allows for the study

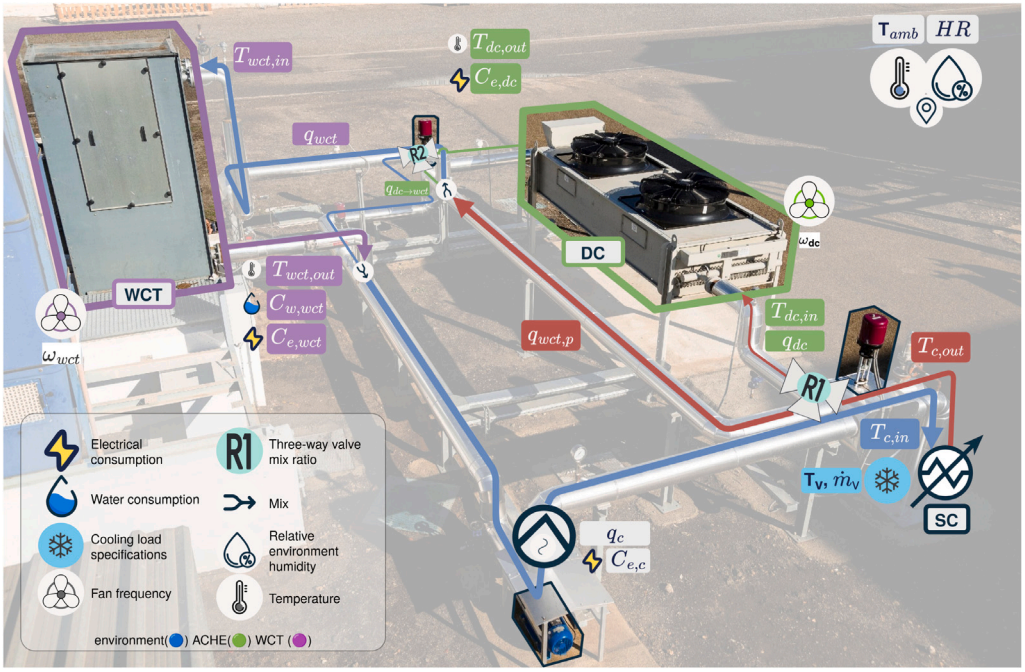

Fig. 1. Combined cooling system facility.

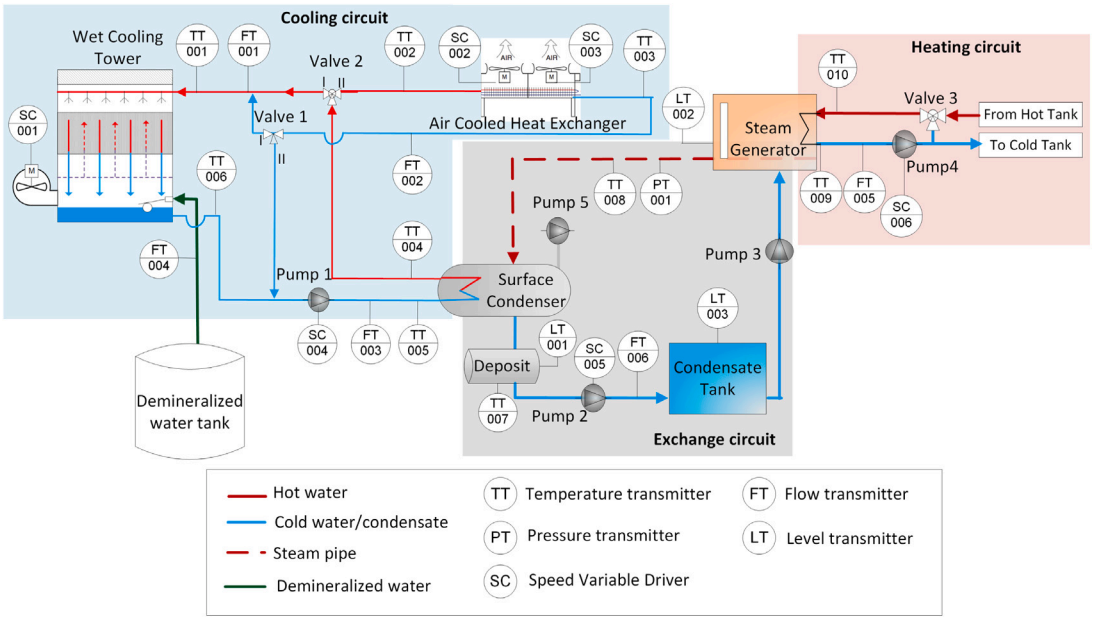

Fig. 2. Layout of combined cooling systems pilot plant.

and validation of different cooling configurations, models, and control and optimization strategies.

This pilot plant consists of three circuits: cooling, exchange, and heating (see the layout in Fig. 2).

In the cooling circuit, water circulates through the tube bundle of a Surface Condenser (SC), which can be cooled via WCT and/or DC (ACHE-type), both with a design thermal power of 204 kW_{th}. The operation of the system can be configured in different modes according to the positions (I/II) of valves 1 and 2 (see Table 1).

In the exchange circuit, a saturated steam generator with a nominal thermal power of 80 kW_{th} produces steam at varying pressures (ranging from 82 mbar to 200 mbar). This steam is subsequently condensed in the surface condenser, thereby transferring its latent heat of condensation to the cooling water, which is heated in the process.

Table 1
Cooling configurations, where I and II represents the positions of valves 1 and 2 in Fig. 2.

Configuration	Valve positions	
	Valve 1	Valve 2
only-DC	II	II
only-WCT	I	–
fully-series	I	II
fully-parallel	(I-II)[a]	II
parallel-series	(I-II)	(I-II)

[a] values between positions I and II

Table 2
Characteristics of instrumentation ([a] value of the temperature in °C, [b] of reading, [c] full scale, [d] mean value).

Measured variable	Instrument	Range	Measurement uncertainty
Water temperature (TT-001... TT-007)	Pt100	0 – 100 °C	$0.03 + 0.005 \cdot T^{a}$
Cooling water flow rate (FT-001...FT-003)	Vortex flow meter	9.8 – 25 m^3/h	± 0.65 % o.r.[b]
Water flow rate (FT-004)	Paddle wheel flow meter	0.05 – 2 m^3/h	± 0.5% of F.S[c] + 2.5% o.r
Condensate water flow rate (FT-006)	Coriolis flow meter	0.1 – 0.3 m^3/h	< 0.1% +
Ambient temperature	Pt1000	−40 – 60 °C	±0.4@20 °C
Relative humidity	Capacitive sensor	0% – 98%	± 3% o.r @20 °C
Air velocity	Impeller anemometer	0.1 – 15 m s^{-1}	±0.1 m s^{-1} + 1.5% o.r
Outlet air temperature	Pt100	−20 – 70 °C	±0.5 °C
Outlet air humidity	Capacitive sensor	0 – 100%	± 2%

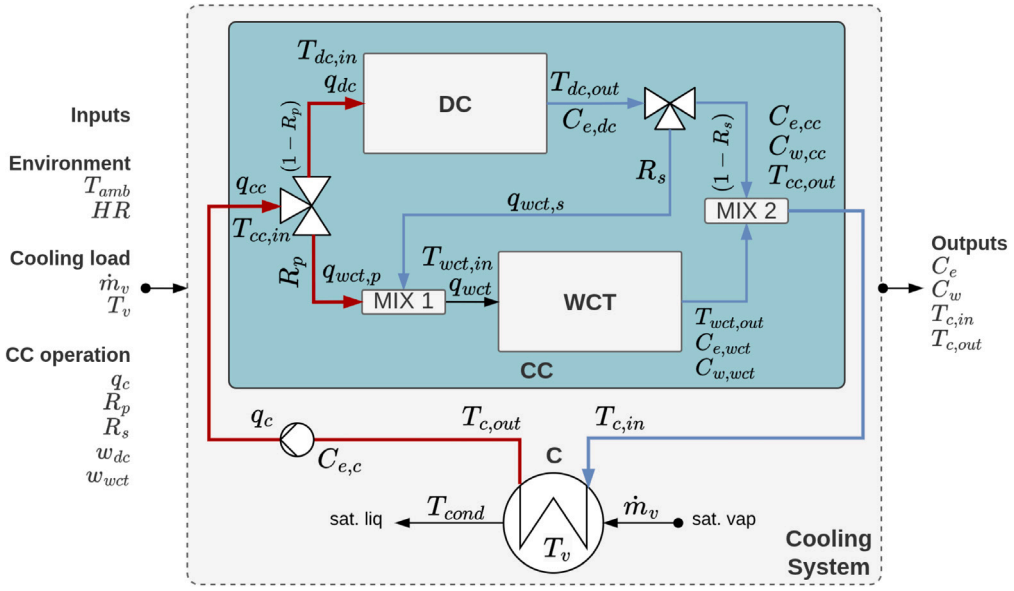

Fig. 3. Diagram of the combined cooling model.

In the heating circuit, a solar field with a thermal power of 300 kW_{th} (at the design point) supplies the necessary energy to the steam generator in the form of hot water.

Instrumentation related to the CC pilot plant is detailed in Table 2. Note that sensors measuring air velocity and temperature at the outlet of the cooling systems have not been permanently installed. Instead, portable sensors were used during specific experiments.

3. Simulation model

In order to study the potential advantages of using a combined cooling system, the modeling of its components must first be developed. As the aim is to predict performance, this section focuses on steady-state modeling of the main components of the combined cooler, *i.e.*, the WCT and the DC, as well as auxiliary components such as the SC, regulation valves, and mixer points.

Fig. 3 shows a diagram of the CC model, which includes the input and output variables described in the Nomenclature.

3.1. Wet cooling tower model

In the case of cooling towers, the Merkel number is a dimensionless parameter widely recognized as a performance key indicator. It is commonly employed in experimental characterization, numerical simulations, and optimization studies. This parameter can be evaluated through several theoretical approaches, including the original Merkel formulation [17], the effectiveness–NTU method [18], and the more comprehensive Poppe model [19].

The Merkel theory is based on a number of simplifying assumptions. Merkel assumed that the air leaving the fill is saturated with water vapor, being characterized only by its enthalpy. Therefore, the state of the air leaving the fill cannot be determined according to this theory. The effectiveness–NTU method of analysis is based on the same simplifying assumptions as the Merkel theory. As a result, the performance predictions obtained from both methods are typically very similar. In the Poppe theory, the governing equations for heat and mass transfer in the exchange area of the cooling tower are derived and simplified. As a result, the evolution of key thermodynamic variables, such as air humidity, air enthalpy, water temperature, and water mass flow rate, can be predicted throughout the fill section.

Several investigations have compared the previously mentioned theories for thermal performance evaluation of wet cooling towers. Some examples include the works of [20–22]. These investigations generally conclude that the Poppe method offers a more accurate representation of the physics of the problem, as it enables the prediction of moist air properties and the quantification of evaporative water losses. Consequently, the Poppe method is recommended for applications in which an accurate determination of the outlet air state is required.

According to the Poppe theory, the major following equations for the heat and mass transfer are obtained:

$$\frac{d\omega}{dT_w} = \frac{c_{p_w} \cdot \dot{m}_w/\dot{m}_a \cdot (\omega_{s_w} - \omega)}{(h_{s_w} - h) + (\mathrm{Le} - 1) \cdot \left[(h_{s_w} - h) - (\omega_{s_w} - \omega) \cdot h_v\right] - (\omega_{s_w} - \omega) \cdot h_w}, \quad (1)$$

$$\frac{dh}{dT_w} = c_{p_w} \cdot \times \frac{\dot{m}_w}{\dot{m}_a} \left[1 + \frac{(\omega_{s_w} - \omega) \cdot c_{p_w} \cdot T_w}{(h_{s_w} - h) + (\mathrm{Le} - 1) \cdot [(h_{s_w} - h) - (\omega_{s_w} - \omega) \cdot h_v] - (\omega_{s_w} - \omega) \cdot h_w}\right], \quad (2)$$

$$\frac{d\,\mathrm{Me}}{dT_w} = \frac{c_{p_w}}{(h_{s_w} - h) + (\mathrm{Le} - 1) \cdot [(h_{s_w} - h) - (\omega_{s_w} - \omega) \cdot h_v] - (\omega_{s_w} - \omega) \cdot h_w}. \quad (3)$$

Please refer to [20–22] for a detailed derivation and simplification of the governing equations. From Eqs. (1), (2) and (3), the evolution of key variables such as the air enthalpy, humidity ratio, and the Merkel number along the fill height is obtained by numerically solving the set of differential equations using a fourth-order Runge–Kutta algorithm.

The Merkel number of a wet cooling tower is not a constant value but varies with the operating conditions. When plotted against the water-to-air mass flow ratio (defined as the ratio between the water and air mass flow rates within the tower) it typically follows a straight, decreasing trend in logarithmic coordinates. As suggested by ASHRAE [23], this behavior is often expressed through a single correlation that depends on the water-to-air mass flow ratio, Eq. (4).

$$\mathrm{Me} = c \cdot \left(\frac{\dot{m}_w}{\dot{m}_a}\right)^{-n} \quad (4)$$

3.2. Dry cooler model

The modeling of air cooled heat exchangers for the simulation of whole power plants can involve different levels of complexity. It is common to assume a constant effectiveness or overall heat transfer coefficient as, for example, the type 5 in the software Trnsys [24]. However, these models cannot consider the effect of relevant operating conditions as the water or air flow rates, which significantly affect the heat transferred and the power consumption.

For preliminary designs, it is common to rely on empirical models, based on experimental correlations available in the open literature [25]. While this option takes into account the operating conditions, the model must be carefully applied out of the range of the operating conditions covered by the original correlations. Additionally, it can be difficult to find correlations for relatively complex geometries. To partially solve these issues, other models adjust some parameters by performing component tests and, at the same time, keep the main physics of the model, e.g., obtaining a Nusselt number correlation for a specific configuration as a function of the Reynolds and Prandtl numbers.

The following simplifying assumptions have been considered to model the DC system in this paper (ACHE-type): steady-state conditions, uniform heat transfer coefficients along the heat transfer surface, uniform water flow distribution in the tubes, uniform flow velocity on the air side, negligible heat losses to the surroundings and the fouling resistances (air and water sides) are neglected.

The equations for a general heat exchanger [26] are applied: heat transferred from the hot fluid (water), heat transferred to the cold fluid (air) and the heat transfer based on the overall heat transfer coefficient and the logarithmic mean temperature difference:

$$\dot{Q}_{dc} = \dot{m}_{dc} \cdot c_{p,c} \cdot (T_{dc,in} - T_{dc,out}), \quad (5)$$

$$\dot{Q}_{dc} = \dot{m}_a \cdot c_{p,a} \cdot (T_{a,out} - T_{amb}), \quad (6)$$

$$\dot{Q}_{dc} = U_{dc} \cdot A \cdot F \cdot \mathrm{LMTD}, \quad (7)$$

where F is the correction factor for the LMTD (Log Mean Temperature Difference), which is calculated for a cross flow heat exchanger with three tube rows and three tube passes [27], and the product of the overall heat transfer coefficient and the heat exchange area is calculated from:

$$U_{dc} \cdot A = \left(\frac{1}{A_i \cdot h_i} + \frac{\ln(D_{tb,o}/D_{tb,i})}{2 \cdot \pi \cdot k_{tb} \cdot L_{tb} \cdot n_{tb}} + \frac{1}{A_o \cdot h_o}\right)^{-1}, \quad (8)$$

Table 3
Main DC features at pilot plant.

Concept	Value	Unit
Number of tubes	60	–
Number of passes per tube	3	–
Tube length	3.6	m
Outer tube diameter	12.7	mm
Inner tube diameter	9.4	mm
Tube material	Copper	–
Fin thickness	0.21	mm
Fin spacing	2.4	mm
Fin material	Aluminum	–

being h_o the convective heat transfer coefficient for the external surface of a single horizontal tube, $D_{tb,o}$ the outer tube diameter, $D_{tb,i}$ the inner tube diameter, k_{tb} the thermal conductivity of the tube wall material, and h_i the convective heat transfer coefficient for the water inside the tube.

The convective heat transfer coefficient on the internal side (cooling water), h_i, is calculated using Gnielinski's correlation [28].

The convective heat transfer coefficient on the external surface (air), h_o, cannot be easily calculated from correlations in the open literature due to the geometry involved (tube arrays with transversal plate fins). Thus, as described in Sections 4 and 5.2, an experimental campaign was performed, covering a wide range of operating conditions, to fit the experimental data to an equation that related the air side Nusselt number and the air side Reynolds number, as follows:

$$\mathrm{Nu}_a = G \cdot \mathrm{Re}_a^m \cdot \mathrm{Pr}_a^{0.36}, \quad (9)$$

where $Nu_a = h_o \cdot L_{tb}/k_{tb}$, and G and m are parameters to be determined by fitting to experimental data, and the exponent for the Prandtl number, Pr, is assumed to be the same value as that proposed by Zukauskas for staggered tube banks [29].

Table 3 presents the main characteristics and design specifications of the DC at the pilot plant.

3.3. Surface condenser model

The surface condenser can be modeled using similar heat balances as in the previous Section. This law states that, under ideal conditions, the heat released as a result of condensation (Eq. (10)) is equal to the heat gained by the cooling water (Eq. (11)) and also to the heat transferred by the condenser heat transfer surfaces (Eq. (12)).

$$\dot{Q}_c = \dot{m}_v \cdot (h_{sat.vap} - h_{sat.liq}) \quad (10)$$

$$\dot{Q}_c = \dot{m}_c \cdot c_p \cdot (T_{c,out} - T_{c,in}) \quad (11)$$

$$\dot{Q}_c = U_c \cdot A \cdot \mathrm{LMTD}, \quad (12)$$

being U_c the overall heat transfer coefficient given by Eq. (13):

$$U_c \cdot A = \left(\frac{1}{A_i \cdot h_i} + \frac{R_{if}}{A_i} + \frac{\ln(D_{tb,o}/D_{tb,i})}{2 \cdot \pi \cdot k_{tb} \cdot L_{tb} \cdot n_{tb}} + \frac{1}{A_o \cdot h_o} + \frac{R_{of}}{A_o}\right)^{-1}, \quad (13)$$

where R_{if} and R_{of} are the fouling resistances (inside and outside, respectively).

The model assumes steady-state regime, uniform heat transfer coefficients along the surface of the condenser, *i.e.*, independent of the position in the tube, known condenser geometry, negligible heat losses to the surroundings, and constant and uniform fouling resistances across the condenser surface.

The shell-side heat transfer coefficient h_o is estimated using the Nusselt method [30] for laminar-flow condensation over a horizontal tube bundle ($0 < Re < 30 \times 10^6$) including the Kern correction for condensate inundation, while the tube-side convective heat transfer coefficient for the water flow inside the tube bundle, h_i, is approximated using the Petukhov-Kirillov-Popov correlation for fully-developed turbulent flow

Table 4
Main features of the surface condenser at the pilot plant.

Concept	Value	Unit
Number of tubes	96	–
Number of passes per tube	4	–
Tube length	3	m
Outer tube diameter	21.34	mm
Tube thickness	2.108	mm
Thermal conductivity of the tube wall	50	W/(m K)
Tube-side inlet pressure	5	bar
Inner tube-side fouling	$1.72{\cdot}10^{-5}$	m^2 K/W
Outer tube-side fouling	$1.72{\cdot}10^{-5}$	m^2 K/W

through smooth circular tubes [31], valid within $0.5 < Pr < 10^6$ and $4000 < Re < 5 \times 10^6$.

Table 4 presents the main physical characteristics and design specifications of the surface condenser, provided by the manufacturer.

3.4. Valves

The two divergent three-way valves are modeled using the distribution ratio R as inputs, so the mass flow rate at the outlets of each valve can be easily estimated as:

$$q_{v,out1} = R \cdot q_{v,in}, \tag{14}$$

$$q_{v,out2} = (1 - R) \cdot q_{v,in}, \tag{15}$$

being R a value in the range [0,1], which implicitly includes the nonlinearities of the valve.

3.5. Mixers

The mixer's outlet flow, $q_{mix,out}$, and temperature, $T_{mix,out}$, can be determined using simple mass and energy balances from its inlet streams, such as described in the following equations:

$$q_{mix,out} = q_{mix,in,1} + q_{mix,in,2}, \tag{16}$$

$$q_{mix,out} \cdot c_p \cdot T_{mix,out} = q_{mix,in,1} \cdot c_p \cdot T_{mix,in,1} + q_{mix,in,2} \cdot c_p \cdot T_{mix,in,2}, \tag{17}$$

where c_p can be assumed to be the same for the mixing temperature differences of this type of system.

3.6. Electrical consumption

The electrical consumption of the cooling pump and WCT and DC fans was modeled using third-order polynomial regressions based on experimental data, as described in [15]:

$$C_e = p_1 \cdot x^3 + p_2 \cdot x^2 + p_3 \cdot x + p_4, \tag{18}$$

where C_e represents electrical consumption (kW) and x is the value applied to the variable frequency drive of the fan (in percentage). The p_i coefficients correspond to a polynomial regression which were calibrated for each component.

4. Experimental campaigns

As reported in [16], to calibrate and validate the WCT model, 19 and 17 test runs, covering a representative range of operating values, were used [32]. To complement this and establish a reliable CC model, new experimental campaigns were carried out. Table 5 summarizes these new experimental campaigns, describing the design of experiments (DoE) employed and indicating the number of tests conducted under steady-state conditions. The ranges of the variables involved in the experiments are also indicated, with those used to define the DoE for each test campaign shown in bold.

In summary, three new experimental campaigns have been conducted at the pilot plant:

- Model calibration data.
  - As air mass flow rate measurements are a specific requirement for the DC model, the $\dot{m}_{air}$-w_{dc} relationship was derived during an experimental campaign (*DC-f*). Air velocity and temperature were measured at 10 different fan speed levels, ranging from 11% to 100% in 10% increments. The ACHE fan area was divided into eight quadrants, and measurements were taken at the center of each quadrant. The recorded values were then averaged to obtain the mean air velocity and temperature, which were used to calculate the air mass flow rate.
  - An experimental campaign for DC (*DC-cal*) was designed and performed to calibrate the Nusselt number correlation as described in Section 3.2. This campaign comprises 27 tests.
  - An experimental campaign for SC (*SC-cal*) was designed and performed to calibrate the global heat transfer coefficient, U_c, as a function of inlet water temperature, $T_{c,in}$ and water flow rate, q_c. This campaign comprises 15 tests.
- Models validation data. The experimental campaigns designed for the thermal models calibration were repeated to validate the models of DC and SC.
- CC model validation. An additional experimental campaign was designed and performed to validate the complete model of the CC system. This campaign comprises 24 tests.

Three performance metrics were calculated to assess the quality of the models' fit to the experimental data: coefficient of determination (R^2), Mean Absolute Error (MAE) and Mean Absolute Percentage Error (MAPE), as described in the following equations:

$$R^2 = 1 - \frac{\sum_{i=1}^{n}(y_i - \hat{y}_i)^2}{\sum_{i=1}^{n}(y_i - \bar{y})^2}, \tag{19}$$

$$\text{MAE} = \frac{1}{n}\sum_{i=1}^{n}\left|y_i - \hat{y}_i\right|, \tag{20}$$

$$\text{MAPE} = \frac{1}{n}\sum_{i=1}^{n}\left|\frac{y_i - \hat{y}_i}{y_i}\right| \times 100\%, \tag{21}$$

where y_i is the measured or observed value for the output variable, in the ith observation, $\hat{y}_i$ is the estimated value of the same variable, n is the total number of observations and $\bar{y}$ is the mean value of the experimental values.

5. Models calibration and validation

5.1. Wet cooling tower

Previous studies have provided a comprehensive thermal characterization of the wet cooling tower (WCT) implemented in the pilot plant [16,33]. The experimental campaign consisted of 19 test runs to calibrate the model, covering a representative range of operating parameters. Based on the collected data, the authors reported the Me $-\dot{m}_w/\dot{m}_a$ relationship shown in Eq. (22). It is important to note that the Merkel number was calculated using the Poppe formulation.

$$\text{Me} = 1.52 \cdot \left(\frac{\dot{m}_w}{\dot{m}_a}\right)^{-0.69} \tag{22}$$

As described in [16], the validation dataset contained 17 tests and the MAE obtained was 0.27 °C and 6.74 l/h for $T_{out,wct}$ and C_w, respectively.

5.2. Dry cooler

The following $\dot{m}_a$-w_{dc} relation was obtained with the *DC-f* dataset

$$\dot{m}_a = 0.30195 \cdot w_{dc} - 1.02179. \tag{23}$$

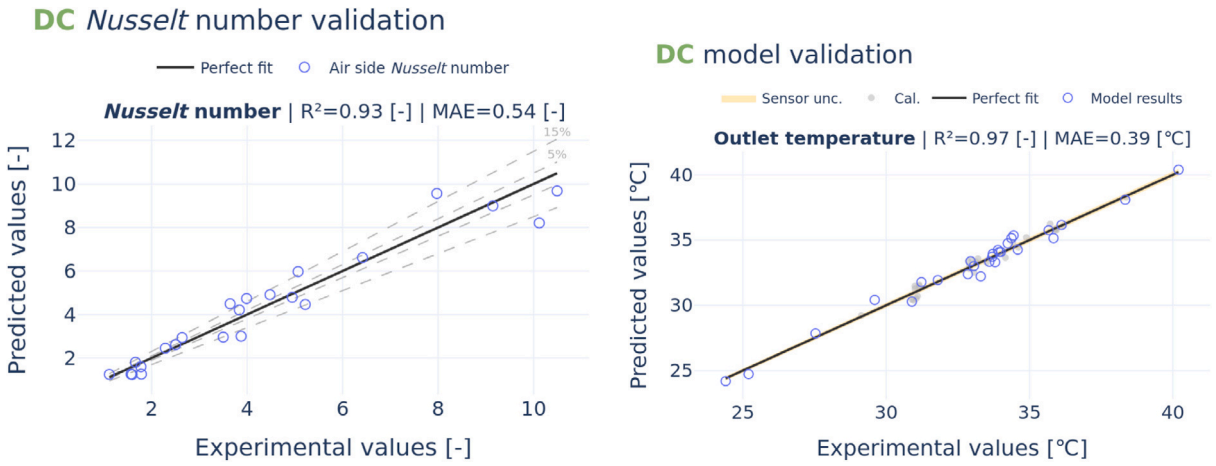

(a) Air side Nusselt number values. (b) Model validation.

Fig. 4. Calibration and validation of DC model.

Table 5
Experimental campaigns performed at the CC pilot plant, where GD-n_1-n_2 refers to the spatial grid distribution (n_1) around the fan with n_2 measurements in each quadrant ($n_1 \times n_2$ measurements); *BB-n_1-n_2* denotes a Box-Behnken design with n_1 variables and n_2 levels; and *FF-n_1-...-n_i* indicates a full factorial design with i variables, each with n_i levels.

Features	Component calibration			Component validation		System validation
	DC-f	DC-cal	SC-cal	DC-val	SC-val	CC-val
DoE	GD-8–10	BB-4–3	BB-3–3	BB-4–3	BB-3–3	FF-2-2-2-3
NumTests	80	27	15	27	15	24
T_{amb} (°C)	26	**12 – 29**	–	**13 – 32**	–	**12 – 37**
HR (%)	–	–	–	–	–	14 – 63
$\dot{m}_v$ (kg/h)	–	–	118 – 328	–	133 – 287	200 – 310
$\dot{Q}_c$ (kW)	–	–	**78 – 216**	–	**88 – 187**	**132 – 202**
q_c (m³/h)	–	–	**10 – 24**	–	**10 – 24**	**18 – 24**
q_{dc} (m³/h)	–	**5 – 25**	–	**5 – 24**	–	**5 - 24**
q_{wct} (m³/h)	–	–	–	–	–	**6 – 24**
$T_{dc,in}$ (°C)	–	**35 – 41**	–	**31 – 42**	–	33 – 54
$T_{dc,in}$ - $T_{dc,out}$ (°C)	–	**2 – 7**		**2 – 9**		1 – 11
T_v (°C)	–	–	**36 – 56**	–	**36 – 56**	**36 – 57**
$T_{wct,in}$ (°C)	–	–	–	–	–	33 – 54
w_{dc} (%)	11 – 100	**11 – 76**	–	**11 – 98**	–	11 – 100
w_{wct} (%)	–	–	–	–	–	21 – 87

The DC model uses this linear function to estimate the air mass flow rate, with the w_{dc} input applied in the pilot plant.

Once the air mass flow rate is established, the set of 27 experimental points (defined as *DC-th* in Table 5) was used to fit the experimental data to Eq. (9). To do so, Eqs. (5) and (8) were used to determine the air side heat transfer coefficient using the inlet and outlet water temperatures, the air inlet temperature, and the mass flow rates for both fluids as known values. The obtained correlation is described as follows:

$$\mathrm{Nu}_a = 0.006411 \cdot \mathrm{Re}_a^{0.9143} \cdot \mathrm{Pr}_a^{0.36}. \quad (24)$$

Fig. 4(a) shows the predicted air side Nusselt number values compared with the actual values. As can be seen, 82% of the data points have a deviation of less than 20%. The straight line represents the perfect fit: the closer the values are to this line, the better the correlation.

Using the previous correlations, Eqs. (5)–(8) and (23)–(24), the DC model can be used to estimate the outlet water temperature, $T_{dc,out}$, using as inputs $\dot{m}_{dc}$, w_{dc}, T_{amb} and $T_{in,dc}$.

A new set of 27 experiments was conducted to validate the previously developed model. Fig. 4 shows the comparison between the predicted and experimental values. The model's performance is evident, with MAE of 0.39 °C.

5.3. Surface condenser

Following the same methodology as in the previous case, a set of 15 experiments was firstly used (*SC-cal* in Table 5) to calculate the global heat transfer coefficient, U_c, with Eq. (8) and the SC specifications. U_c is in this case calibrated as a function of the input variables $T_{c,in}$ and q_c, obtaining the following relation:

$$U_c = p_1 \cdot T_{c,in} + p_2 \cdot \dot{m}_{c,tb} + p_3 \cdot \dot{m}_{c,tb} \cdot T_{c,in} + p_4 + p_5 \cdot \dot{m}_{c,tb}^2 + p_6 \cdot T_{c,in}^2, \quad (25)$$

where $\dot{m}_{c,tb}$ is the water mass flow rate inside each condenser tube, p_1=12.71, p_2=2.91, p_3=9.5 $\cdot 10^{-3}$, p_4=343.29, p_5=-1 $\cdot 10^{-3}$ and p_6=-4.83 $\cdot 10^{-2}$, where each parameter, p_i has units consistent with the variables involved.

Using the previous relation and Eqs. (10)–(12), the surface condenser model can be solved to estimate $T_{c,\mathrm{out}}$ and T_v, assuming that the water leaving the shell side of the condenser is saturated at temperature T_v. In this case the inputs of the model are $T_{c,in}$, $\dot{m}_c$ and $\dot{m}_v$.

To validate this model, a different data set of 15 steady state tests (*SC-val* in Table 5) has been used with the results depicted in Fig. 5. The predicted outlet water temperature in the tubes shows good agreement with the experimental measurements, with a low MAE. In contrast, the prediction error is larger for the condensate water temperature at the shell-side outlet (MAE = 1.86 °C). This discrepancy may arise because

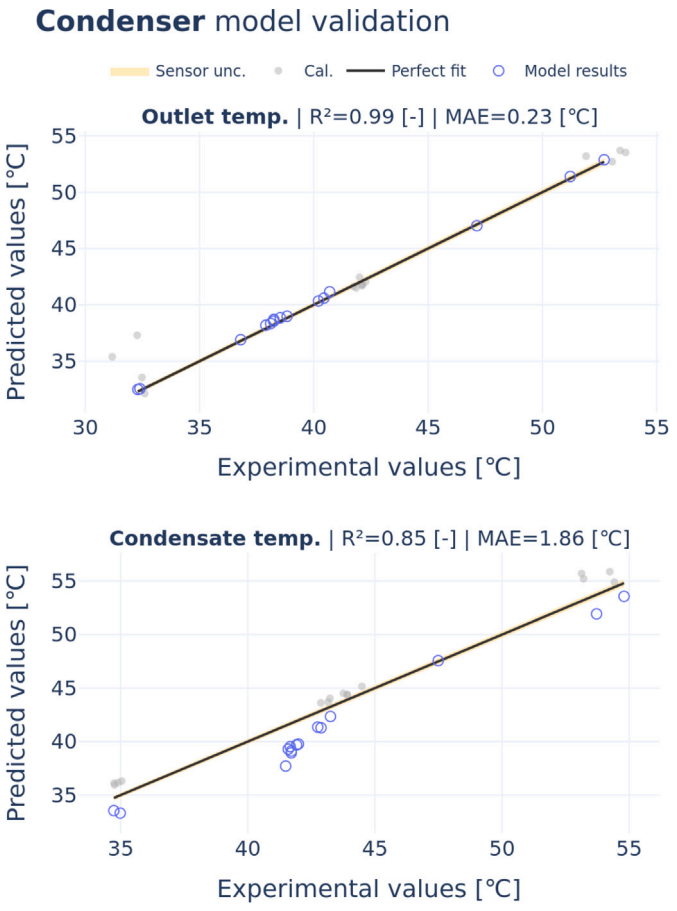

Fig. 5. Surface condenser validation.

the experimental outlet temperature does not exactly match the vapor saturation temperature (T_v), but is instead 0.1 to 1.7 °C subcooled.

5.4. Combined cooler

The complete model of the combined cooler has been validated with a different dataset composed of 24 tests (*CC-val* in Table 5). Fig. 6 compares the experimental results with the predicted values using as input variables those defined in Fig. 3 . To visualize the operational characteristics of each test, the data points are represented with the following information:

- The dashed circle represents the nominal cooling power (200 kW_{th}).
- The filled circle represents the cooling power measured in the test relative to the nominal value. The closer it is to the dashed circle, the closer the cooling power is to the nominal one.
- The measured cooling power is achieved using a certain percentage of DC and WCT. These contributions are distinguished by green and purple, respectively. For example, if the ring is mostly green, it reflects that the cooling contribution from DC is predominantly larger than that from WCT.
- The filling color inside the circle represents the ambient temperature. From low temperature (no filling) to high ambient temperature (dark yellow).

With this representation, it can be observed that the CC model provides satisfactory results over a wide range of operating and ambient conditions. The temperatures related to DC, WCT and SC show a MAE lower than 0.97 °C, with the largest error occurring in $T_{wct,out}$, when the cooling power was far from the nominal value. This may be due to the need to improve the relation $\dot{m}_{air}-w_{wct}$ relationship at low flow rates. In the case of water consumption, the trend of the predicted values follows that of the experimental data, although with a higher discrepancy (R^2=0.82), with the MAE being 19.4 l/h. The results suggest that the error is not related to ambient temperature, cooling configuration, or thermal cooling requirements.

Table 6
Performance metrics obtained with the CC models (*s.u.* means same units as predicted variable).

Predicted variable	Performance metric					
	R^2 (-)		MAE (s.u.)		MAPE (%)	
	Cnt	CC	Cnt	CC	Cnt	CC
$T_{dc,out}$ (°C)	0.99	0.98	0.29	0.46	0.90	1.17
$T_{wct,out}$ (°C)	0.92	0.94	1.01	0.97	3.01	2.72
C_w (l/h)	0.87	0.82	16.55	19.40	10.42	11.03
$T_{c,out}$ (°C)	0.98	0.99	0.23	0.41	1.51	1.00
$T_{c,in}$ (°C)	–	0.99	–	0.53	–	1.52

A summary of the models' results using dataset *CC-val* is shown in Table 6. This table includes the performance metrics of each component simulated individually (*Cnt* column) and those obtained with the complete model (*CC* column). The performance metrics obtained validate the model and provide the opportunity of using it for the analysis of the CC technology under different cases of study.

6. Optimization analysis

After the validation process, the CC model was used to analyze the potential of applying optimization algorithms to improve the operation of cooling systems in CSP plants. The primary objective of the cooling system is to condense all incoming saturated vapor into saturated liquid, thereby fulfilling the cooling requirements. To achieve this, the system relies on two resources: electricity and water. Due to the inherent characteristics of the process, the consumption of these resources follows conflicting trends, making the problem inherently a case of multi-objective optimization. Consequently, there is no single optimal solution; instead, a set of equally viable solutions exists; the Pareto front region [34,35], representing a trade-off between the objectives.

A straightforward approach to solve the multi-objective optimization problem is to do a grid-search over the decision space, that is, evaluating the model for every combination of decision variables and validating that they produce feasible solutions. The selected decision variables are related to the operation of the cooling system: hydraulic configuration (R_p, R_s), the cooling provided by each component (represented by its fan speeds, ω_d, ω_{wct}) and the coolant recirculation flow (q_c). The problem can be formally defined as follows:

$$\min_{u} \quad J = f(C_w, C_e) \tag{26}$$

$$\text{s.t.} \quad T_v = T_v^* \tag{27}$$

$$\text{with} \quad u = [\, q_c,\ R_p,\ R_s,\ \omega_{\text{dc}},\ \omega_{\text{wct}} \,], \tag{28}$$

where T_v^* is the established value for the vapor temperature, which is assumed to be the temperature of the water leaving the shell side of the condenser. It is important to note that this optimization problem considers only the cooling system and not the connected process. If the performance of the CSP plant were included in the optimization problem, the temperature of the condensate water leaving the shell side of the surface condenser would become an additional decision variable, as it would affect the cycle thermal performance.

Next, the Pareto front is determined from the set of feasible points, evaluated in terms of the two consumptions: electricity (C_e) and water (C_w). By definition, the Pareto front consists of solutions where no objective can be improved without worsening the other. To identify it, each feasible point is compared against all others: if a point is

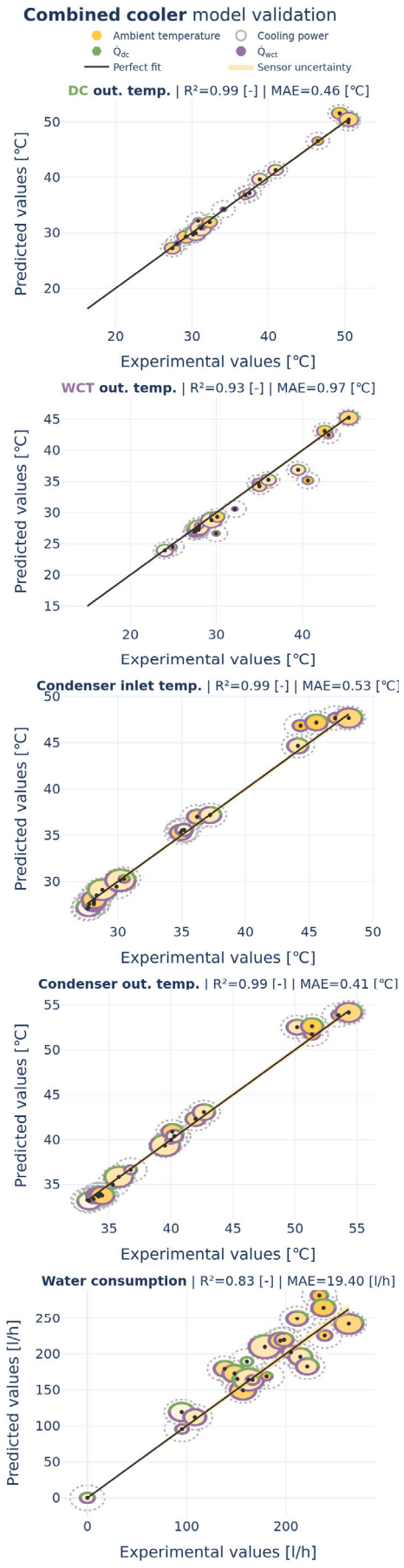

Fig. 6. CC validation.

dominated, that is, another point performs better in both objectives, it is excluded. The remaining non-dominated points form the Pareto front.

Four case studies (see Table 7) have been analyzed through simulation, each undergoing an optimization process. The cooling power demand was varied using a thermal load (TL) factor at two levels: nominal operating conditions (200 kW_{th}), corresponding to a TL of 100 %, and a partial load condition at 60 % TL. For each cooling load, the impact of environmental conditions on system performance was assessed. Specifically, typical summer (ambient temperature = 30 °C, relative humidity = 40 %) and winter (ambient temperature = 10 °C, relative humidity = 70 %) conditions in the location of Tabernas (Almería, Spain) were considered. Additionally, the temperature of the vapor was set at 42 °C.

The upper plot in Fig. 7 shows the Pareto fronts obtained for the four case studies. Each point is associated with specific values that define the operating configuration (q_c, R_p, R_s, $T_{dc,out}$, $T_{wct,out}$), the decision variables in the optimization procedure. A point with zero water consumption represents only-DC operation, while a point with minimum electricity consumption represents only-WCT operation. The remaining points correspond to combined configurations.

In Case I, which presents the highest water and electricity consumptions, it is observed that water consumption always exceeds 100 l/h. This indicates that the use of the WCT is essential, as the DC alone is not capable of cooling 200 kW_{th} of vapor at 42 °C under summer conditions. If the system operated only with the DC, the vapor temperature (*i.e.*, turbine backpressure) would increase, negatively impacting the power cycle performance of a CSP plant. Maintaining the same ambient conditions, when the thermal power is reduced (Case II), it becomes feasible to operate only with DC, although with a high electricity consumption of 7.4 kW_e. By combining DC with WCT, electricity consumption can be reduced by half, with water consumption remaining below 50 l/h. Under more favorable winter conditions (Cases III and IV), the DC alone becomes more efficient as demonstrated by the significant reduction in electricity demand. Still, when coupled with the WCT, electricity consumption can decrease by about 35 % at full thermal load (TL 100 %), with a limited water consumption of 50 l/h. At reduced thermal load (TL 60 %) the additional benefit of the WCT becomes negligible, making this the only case where operating with DC alone is more favorable.

Some detailed results from Case III are represented in the bottom part of Fig. 7. The green and purple areas correspond to the use of DC and WCT, respectively. To avoid water consumption, steam must be cooled exclusively using the DC (zero water consumption in x-axis). At the other extreme of the *x*-axis, the only-WCT operation is represented. At intermediate optimal points, both systems are combined. This is achieved through parallel-series configurations that prioritize dry cooling (for low water consumption in the x-axis) and progressively increase the use of WCT. As expected, the cooling water flow rate (Fig. 7 - *Hydraulic distribution*) is higher (17 m^3/h) for a DC operation, since the reduced temperature component of the cooling driving force is limited and therefore needs to be compensated with a higher flow. It is higher compared to the WCT operation due to its inherently higher temperature difference, allowing for a better (lower) flow of 10 m^3/h. In Fig. 7 - *Cooling power distribution* it is also interesting to highlight how the series-parallel flexibility of the system enables it to achieve almost a continuous division of the cooling power from only-DC to only-WCT, at least for this particular case.

7. Conclusions

This paper takes an important step toward reliable studies of combined cooling systems for CSP plants. It proposes a combined cooling technology that integrates dry cooling and wet cooling towers. The system shows promise and is being further investigated to assess its commercial feasibility for CSP applications.

Table 7
Cases of study.

Case	TL (%)	T (°C)	HR (%)
1	100	30	40
2	60		
3	100	10	70
4	60		

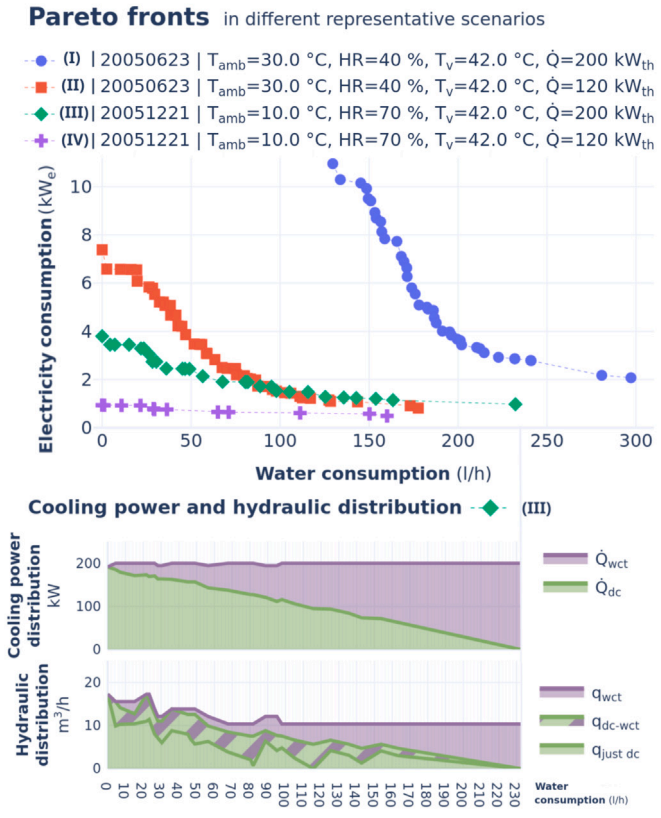

Fig. 7. Pareto fronts in different representative scenarios.

To support this goal, a physical model of the combined cooling system was developed and validated using data from a pilot plant. The model achieved mean absolute errors below 0.97 °C (3.0 % MAPE) for temperatures and 19.4 l/h (10.4 % MAPE) for water consumption, demonstrating its reliability and accuracy.

The model was then used in an optimization process to identify the WCT–DC configuration that minimizes both electricity and water use. Four case studies, covering different seasons and thermal loads, were analyzed. For instance, in summer conditions, WCT operation is essential to maintain vapor temperatures near desired values (close to ambient temperature conditions). However, relying solely on WCT leads to high water consumption— around 300 l/h for a 200 kW_{th} load, or 170 l/h for 120 kW_{th}. Combining WCT with DC in a parallel–series setup allows flexible operation depending on water availability, significantly reducing consumption through partial DC use.

The developed model and optimization framework offer a solid foundation for further studies. They can be readily adapted to commercial CSP plants and used to compare combined cooling performance against conventional systems.

CRediT authorship contribution statement

Juan Miguel Serrano: Writing – review & editing, Writing – original draft, Visualization, Software. **Patricia Palenzuela:** Writing – review & editing, Validation, Supervision, Investigation, Conceptualization. **Javier Ruiz:** Writing – review & editing, Supervision, Methodology, Conceptualization. **Pedro Navarro:** Writing – original draft, Validation, Software, Methodology. **José Muñoz-Cámara:** Writing – original draft, Validation, Software, Methodology. **Bartolomé Ortega-Delgado:** Writing – original draft, Software, Methodology. **Lidia Roca:** Writing – review & editing, Writing – original draft, Supervision, Methodology, Investigation, Funding acquisition, Data curation, Conceptualization.

Declaration of competing interest

The authors declare that they have no known competing financial interests or personal relationships that could have appeared to influence the work reported in this paper.

Acknowledgments

This publication is part of the R&D project PID2021-126452OA-I00, funded by MCIN/AEI/10.13039/501100011033/ and "ERDF A way of making Europe". The authors thank the Plataforma Solar de Almería for providing access to its facilities.

Data availability

All data will be made available in open access at: 10.5281/zenodo.17312546.

References

[1] Maulbetsch J. Comparison of alternate cooling technologies for U.S. power plants: economic, environmental, and other tradeoffs. Tech. rep. 1005358, Palo Alto, CA: EPRI; 2004.
[2] Maulbetsch J. Economic evaluation of alternative cooling technologies. Tech. rep. 1024805, Palo Alto, CA: Electric Power Research Institute (EPRI); 2012.
[3] Tang T, Xu J-q, Jin S-x, Wei H-q. Study on operating characteristics of power plant with dry and wet cooling systems. Energy Power Eng 2013;5(4):651–6. http://dx.doi.org/10.4236/epe.2013.54B126.
[4] Barigozzi G, Perdichizzi A, Ravelli S. Performance prediction and optimization of a waste-to-energy cogeneration plant with combined wet and dry cooling system. Appl Energy 2014;115:65–74. http://dx.doi.org/10.1016/j.apenergy.2013.11.024.
[5] Hu H, Li Z, Jiang Y, Du X. Thermodynamic characteristics of thermal power plant with hybrid (dry/wet) cooling system. Energy 2018;147:729–41. http://dx.doi.org/10.1016/j.energy.2018.01.074.
[6] Wagner MJ, Kutscher C. The impact of hybrid wet/dry cooling on concentrating solar power plant performance. In: ASME 2010 4th international conference on energy sustainability. American Society of Mechanical Engineers Digital Collection; 2010, p. 675–82. http://dx.doi.org/10.1115/ES2010-90442.
[7] Asfand F, Palenzuela P, Roca L, Caron A, Lemarié C-A, Gillard J, Turner P, Patchigolla K. Thermodynamic performance and water consumption of hybrid cooling system configurations for concentrated solar power plants. Sustainability 2020;12(11). http://dx.doi.org/10.3390/su12114739.
[8] Cutillas CG, Ruiz J, Asfand F, Patchigolla K, Lucas M. Energetic, exergetic and environmental (3E) analyses of different cooling technologies (wet, dry and hybrid) in a CSP thermal power plant. Case Stud Therm Eng 2021;28:101545. http://dx.doi.org/10.1016/j.csite.2021.101545.
[9] Ruiz J, Gascó C, Opolot M, Hooman K. Performance evaluation of natural draft dry cooling towers and pre-cooled natural draft dry cooling towers in concentrated solar power plants. Energy 2025;333:137362. http://dx.doi.org/10.1016/j.energy.2025.137362.
[10] Mdallal A, Haridy S, Mahmoud M, Alami AH, Olabi AG, Abdelkareem MA. Modelling and optimization of concentrated solar power using response surface methodology: A comparative study of air, water, and hybrid cooling techniques. Energy Convers Manage 2024;319:118915. http://dx.doi.org/10.1016/j.enconman.2024.118915.

[11] Fernández-Torrijos M, Marugán-Cruz C, Sobrino C, Santana D. The water cost effect of hybrid-parallel condensing systems in the thermo-economical performance of solar tower plants. Appl Therm Eng 2022;202:117801. http://dx.doi.org/10.1016/j.applthermaleng.2021.117801.
[12] SPX. SPX awarded contract to supply parallel condensing system for crescent dunes solar energy project near Tonopah, Nevada. 2012, https://www.powersystemsdesign.com/articles/spx-awarded-contract-to-supply-parallel-condensing-system-for-crescent-dunes-solar-energy-project-near-tonopah-nevada/8/3720.
[13] Asvapoositkul W, Kuansathan M. Comparative evaluation of hybrid (dry/wet) cooling tower performance. Appl Therm Eng 2014;71(1):83–93. http://dx.doi.org/10.1016/j.applthermaleng.2014.06.023.
[14] 2i GmbH S. Blog #29 – full scale testing in stellenbosch, South Africa | minwatercsp. 2020.
[15] Palenzuela P, Roca L, Asfand F, Patchigolla K. Experimental assessment of a pilot scale hybrid cooling system for water consumption reduction in CSP plants. Energy 2022;242:122948. http://dx.doi.org/10.1016/j.energy.2021.122948.
[16] Serrano JM, Navarro P, Ruiz J, Palenzuela P, Lucas M, Roca L. Wet cooling tower performance prediction in CSP plants: A comparison between artificial neural networks and poppe's model. Energy 2024;303:131844. http://dx.doi.org/10.1016/j.energy.2024.131844.
[17] Merkel F. Verdunstungskühlung. VDI Zeitschriff Dtsch Ingenieure Berlin Alemania 1925;123–8.
[18] Jaber H, Webb RL. Design of cooling towers by the effectiveness-NTU method. J Heat Transf 1989;111(4):837–43. http://dx.doi.org/10.1115/1.3250794.
[19] Poppe M, Rögener H. Berechnung von rückkühlwerken. In: VDI Wärmeatlas. 1991, p. Mi 1.
[20] Navarro P, Ruiz J, Hernández M, Kaiser AS, Lucas M. Critical evaluation of the thermal performance analysis of a new cooling tower prototype. Appl Therm Eng 2022;213:118719. http://dx.doi.org/10.1016/j.applthermaleng.2022.118719.
[21] Kloppers J. A critical evaluation and refinement of the performance prediction of wet-cooling towers (Ph.D. thesis), Stellenbosch, South Africa: University of Stellenbosch; 2003.
[22] Kloppers J, Kröger D. A critical investigation into the heat and mass transfer analysis of counterflow wet-cooling towers. Int J Heat Mass Transfer 2005;48(3):765–77. http://dx.doi.org/10.1016/j.ijheatmasstransfer.2004.09.004.
[23] Ashrae. HVAC systems and equipment. In: Chapter 36 cooling towers. 2004.
[24] Klein S. TRNSYS-a transient system simulation program. 2017, Solar Energy Laboratory, University of Wisconsin-Madison.
[25] Zhang W, Ma L, Jia B, Zhang Z, Liu Y, Duan L. Optimization of the circulating cooling water mass flow in indirect dry cooling system of thermal power unit using artificial neural network based on genetic algorithm. Appl Therm Eng 2023;223:120040. http://dx.doi.org/10.1016/j.applthermaleng.2023.120040.
[26] Yunus A Cengel, Afshin J Ghajar. Heat and Mass Transfer. London: McGraw-Hill Professional; 2014.
[27] Kröger D. Air-Cooled heat exchangers and cooling towers. Air-cooled heat exchangers and cooling towers, (v. 1). Penwell Corporation; 2004.
[28] Volker Gnielinski. New equations for heat and mass transfer in turbulent pipe and channel flow. Int Chem Eng 1976;16(2):359–67.
[29] Kakac S, Shah RK, Aung W. Handbook of Single-Phase Convective Heat Transfer. New York, NY, United States: John Wiley and Sons Inc.; 1986.
[30] Serth RW. Process heat transfer: principles, applications and rules of thumb. 2007, http://dx.doi.org/10.1016/B978-0-12-373588-1.X5000-1.
[31] Rohsenow W, Hartnett J, Cho Y. Handbook of Heat Transfer. Third ed.. 1998.
[32] Palenzuela P, Roca L, Serrano JM. Steady-state operation dataset of an experimental wet cooling tower pilot plant located at plataforma solar de almería. 2024, http://dx.doi.org/10.5281/zenodo.10806201.
[33] Navarro P, Serrano J, Roca L, Palenzuela P, Lucas M, Ruiz J. A comparative study on predicting wet cooling tower performance in combined cooling systems for heat rejection in CSP plants. Appl Therm Eng 2024;253:123718. http://dx.doi.org/10.1016/j.applthermaleng.2024.123718.
[34] Censor Y. Pareto optimality in multiobjective problems. Appl Math Optim 1977;4(1):41–59. http://dx.doi.org/10.1007/BF01442131.
[35] Gendreau M, Potvin J-Y, editors. Handbook of metaheuristics. International series in operations research & management science, vol. 146, Boston, MA: Springer US; 2010, http://dx.doi.org/10.1007/978-1-4419-1665-5.